

# Towards 10-nm Soft X-Ray Zone Plate Fabrication

A. Holmberg, J. Reinspach, M. Lindblom, E. Chubarova, M. Bertilson,  
O. von Hofsten, D. Nilsson, M. Selin, D. Larsson, P. Skoglund,  
U. Lundström, P. Takman, U. Vogt, and H. M. Hertz

*Biomedical and X-Ray Physics, Royal Institute of Technology,  
Roslagstullsbacken 21, 10691 Stockholm, Sweden*

**Abstract.** In this paper the latest efforts to improve our nanofabrication process for soft x-ray zone plates is presented. The resolving power, which is proportional to the smallest outermost zone width of the zone plate, is increased by introducing cold development of the electron beam resist that is used for the patterning. With this process we have fabricated Ni zone plates with 13-nm outermost zone and shown potential for making 11-nm half-pitch lines in the electron beam resist. Maintaining the diffraction efficiency of the zone plate is a great concern when the outermost zone width is decreased. To resolve this problem we have developed the so-called Ni-Ge zone plate in which the zone plate is build up by Ni and Ge, resulting in an increase of the diffraction efficiency. In a proof-of-principle experiment with 25-nm Ni-Ge zone plates, we have shown a doubling of the diffraction efficiency. When combined with cold development, the Ni-Ge process has been shown to work down to 16-nm half-pitch. It is plausible that further refinement of the process will make it possible to go to 10-nm outermost zone widths.

**Keywords:** Zone plate, electron beam lithography, electroplating

**PACS:** 07.85.-m, 07.85.Tt, 41.50.+h

## INTRODUCTION

Zone plates are diffractive optical elements commonly used for focusing and imaging in the x-ray spectral range. One example, where a zone plate is used as an objective lens, is soft x-ray (2-4 nm wavelength) microscopy with applications in material, environmental, and life science [1]. In this paper we describe our recent fabrication process developments for these novel nanofabricated lenses.

The zone plate is a circular diffraction grating with alternating transparent and opaque (and/or phase shifting) zones, where the period of the zones decreases from the center to the outer part of the lens. Two of the most important parameters for the zone plate are its outermost zone width ( $dr_N$ ) and its zone height. The resolving power of the zone plate is proportional to  $dr_N$ , and it is therefore desirable to fabricate as small a  $dr_N$  as possible. The zone height will determine the diffraction efficiency of the zone plate, i.e., the amount of incident x-rays that are focused into a certain diffraction order. For soft x-ray wavelengths, Ni and Ge are good optic materials since their phase shift properties result in high efficiency. Figure 1 shows the first-order diffraction efficiency for these materials at  $\lambda = 2.88$  nm as a function of zone height. Throughout the rest of this paper it is the first diffraction order that is considered when the diffraction efficiency is discussed. As can be seen, the maximum efficiency is obtained for a Ni height of  $\sim 200$  nm. However, in practice, nanofabrication problems limit the achievable aspect ratio, and, thus, real zone plates typically have lower heights. This is especially true for zone plates with very small outermost zone widths. For the highest resolution soft x-ray zone plates reported with  $dr_N = 12$  nm [2], the zone height was 30 nm, and consequently the diffraction efficiency is low.

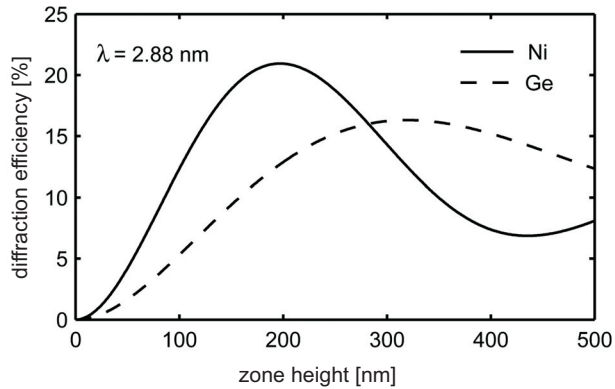


**FIGURE 1.** The first-order diffraction efficiency of a zone plate made in Ni and Ge plotted as a function of zone height.

In this paper we present the latest development in our nanofabrication processes that was made to improve both the resolving power and diffraction efficiency of soft-x-ray zone plates. First, the cold development process that was introduced to increase the resolution in the electron beam resist used for patterning is presented. Then, the new process for fabricating so-called Ni-Ge zone plates is shown. The process combines the electroplating-based Ni process with a subsequent Ge plasma-etch process that can double the diffraction efficiency of a zone plate. This latter process is promising for preserving the diffraction efficiency while the minimum outermost zone widths are pushed towards 10 nm.

### COLD DEVELOPMENT FOR 13-nm ZONE PLATES

The high-resolution nanofabrication process that utilizes cold development is outlined in Fig. 2. The process is similar to our standard process [3] that is used to fabricate zone plates with  $dr_N$  in the 20- to 50-nm range. More details of the cold development process that is presented here can be found in Ref. [4].

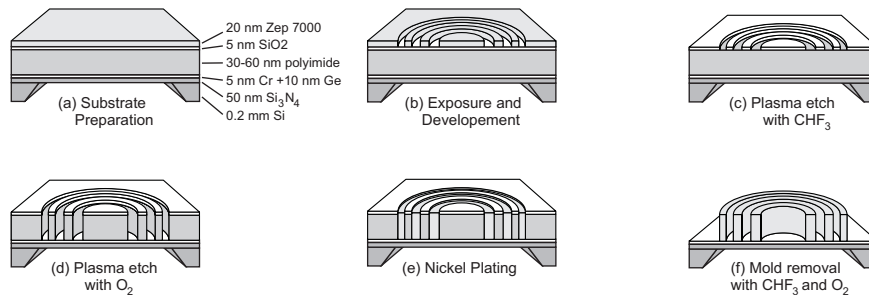


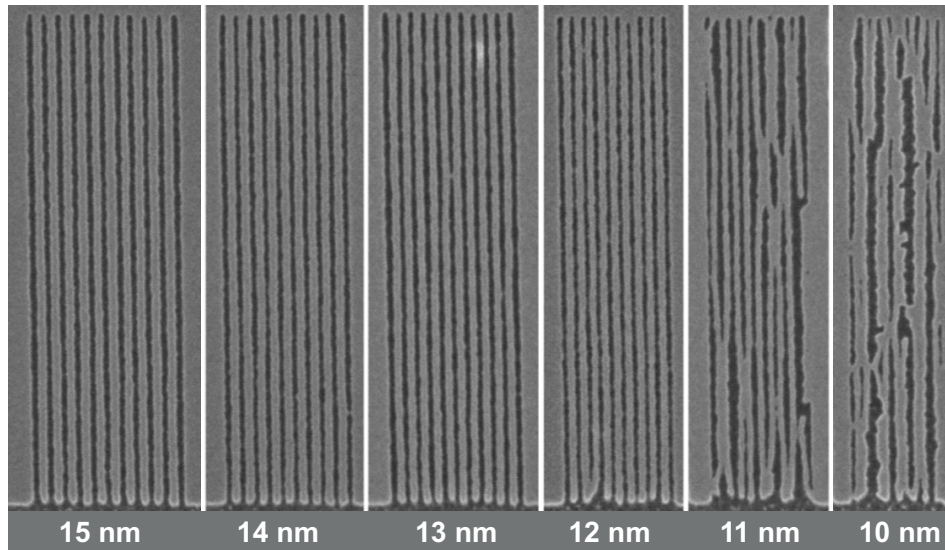
**FIGURE 2.** Nanofabrication process for high-resolution Ni zone plates.

In the first step of the fabrication process, a tri-layer resist mask with plating base is placed on a 50-nm-thick x-ray transmissive  $\text{Si}_3\text{N}_4$  membrane. The plating base consists of a 5-nm Cr sticking layer and a 10-nm Ge electroplating seed layer. On top of this, 30- to 60-nm polyimide (PI-2610, HD Microsystems), a 5-nm  $\text{SiO}_2$  hardmask, and a 20-nm Zep 7000 EBL resist (Zep 7000, Zeon Chemicals, L. P.) form the tri-layer resist. The plating base is deposited by electron-beam evaporation (Edwards Auto 306 system), and the hardmask by rf sputtering (AJA Orion system). The polyimide and the Zep layers are spincoated and baked at 200 °C for 2 h, and at 170 °C for 30 min, respectively.

The patterning of the zone plate then starts with the EBL exposure at 25 keV (Raith 150 system) with a typical dose of  $300 \mu\text{C}/\text{cm}^2$ . The development is then done for 30 s in hexyl acetate cooled to -50 °C followed by a room-temperature rinse for 5 s in isopropyl alcohol and for 3 s in pentane. The developed pattern is transferred into the hardmask by plasma etching (Oxford Plasmalab 100 system) in  $\text{CHF}_3$  for 40 s using 25-W sample rf power, 10-

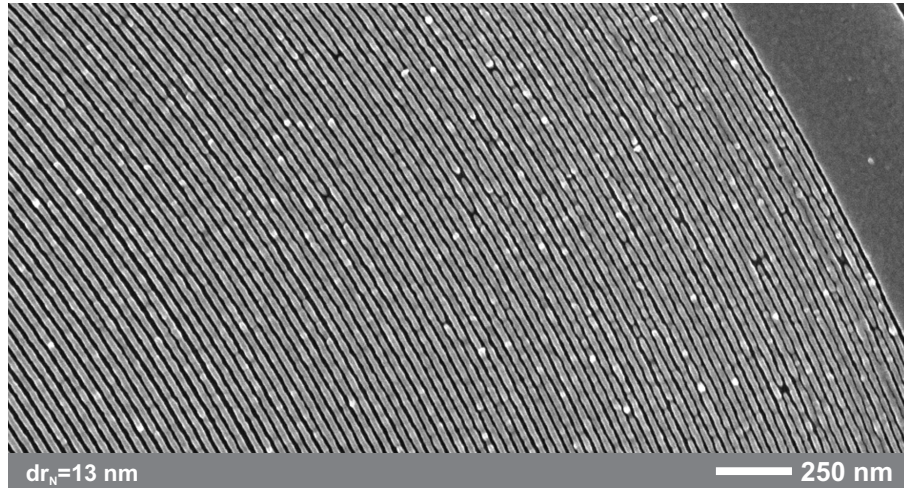
mTorr pressure, and 10-sccm gas flow. Thereafter the pattern is further transferred into the polyimide by plasma etching in  $O_2$  for 1-2 min (depending on the thickness) using 50-W sample rf power, 3-mTorr pressure, and 10-sccm gas flow. The mold is now completed and ready to be filled by electroplating. This is done in a Ni-sulfamate bath (Enthone Inc., LECTRO-NIC 10-03s), which is operated at pH 3.25, 52 °C, and a plating rate of ~30 nm/min. As a final step, the mold is removed by  $CHF_3$  and  $O_2$  etching with the same parameters as for the mold preparation. This results in the final Ni zone plate on the  $Si_3N_4$  membrane with plating base.

Figure 3 shows the best experimental resolution-test result that has been achieved with the cold development process. Scanning electron microscopy (SEM) images of gratings with half-pitch from 15 nm down to 10 nm is shown. The image is taken after the pattern transfer via the  $SiO_2$  hardmask into the polyimide; i.e., the images are taken after finishing the mold as illustrated in Fig. 2(d). The layer thicknesses in this case were: 20-nm Zep7000, 5-nm  $SiO_2$ , and 30-nm polyimide. For the gratings with half-pitch down to 12 nm, the lines are continuous and without defects. Even the 11-nm lines are, apart from some minor defects, well resolved; but the lines have tilted together thus disturbing the look of the grating. The 10-nm half-pitch grating, however, is not resolved in this experiment. Even if the process has been optimized to reach this result, there is still room for improvement in terms of repeatability. A half-pitch down to 13 nm can routinely be produced, but the quality drops quickly for smaller pitch. We believe that the stability of the process can be increased by better control of the thicknesses of the materials in the tri-layer and with an improved experimental arrangement for the cold development. These improvements may also lead to the possibility of making 10-nm half-pitch or smaller without any other changes in the process.



**FIGURE 3.** SEM images illustrating the resolution capabilities with the cold development process. Gratings with half-pitch from 15 to 10 nm are shown.

The complete cold development process has been used to fabricate Ni zone plates with 15, 14, and 13 nm. This should be compared to our best results with room temperature development, which is 20 nm. An SEM image of the outermost part of a  $dr_N = 13$  nm zone plate is shown in Fig. 4. The zone plate has a diameter of 19  $\mu m$ , a focal length of 100  $\mu m$  (@  $\lambda = 2.48$ ), and a Ni thickness of 35 nm.



**FIGURE 4.** The outermost part of a Ni zone plates with 13-nm outermost zone.

Diffraction efficiency measurements have been done in our in-house laboratory laser-plasma-based arrangement [5] that is operated at  $\lambda = 2.88$  nm. The measurements have so far only been possible for  $dr_N = 15$  nm zone plates with longer focal length. This limitation is only due to the present design constraints in the experimental setup. The zone plate parameters for the measured zone plates were: 26- $\mu\text{m}$  diameter, 55-nm zone height, and 135- $\mu\text{m}$  focal length (@  $\lambda = 2.88$  nm). For the best zone plate,  $2.4 \pm 0.4\%$  diffraction efficiency was measured, which is  $\sim 50\%$  of the theoretical efficiency for a zone height of 55 nm.

## NI-GE ZONE PLATES

To improve the diffraction efficiency of the high-resolution zone plates, we have developed the so-called Ni-Ge zone plate [6]. In this process a Ni zone plate is first fabricated as described above (cf. Fig. 2) but on a thicker Ge layer. After the completion of the zone plate, it is used as a mask for a dry etch into the Ge. This new process step can without any compromise be added to the standard Ni process; i.e., the best effort can be made to optimize the Ni zone plate in terms of resolution and diffraction efficiency. The Ge etch is just an additional step that further improves the diffraction efficiency.

An illustration of the additional process step and a graph showing the improvement in efficiency is shown in Fig. 5. The theoretical diffraction efficiencies at  $\lambda = 2.88$  nm are plotted as a function of the Ni thickness for three fixed Ge thicknesses. As can be seen in the graph, the efficiency increase due to the added Ge is significant for Ni thicknesses up to about 100 nm. As typical reproducible aspect ratios are 4:1-5:1 for pure Ni zone plates, a considerable improvement in efficiency can be obtained for Ni-Ge zone plates with zone widths of about 25 nm and below.

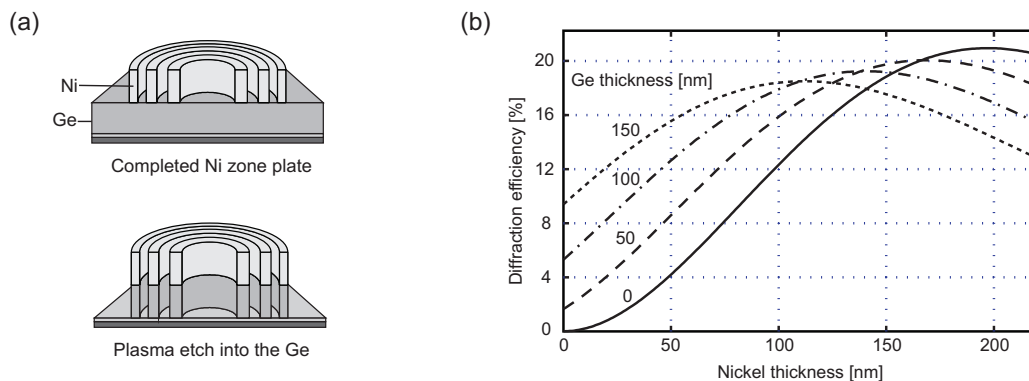


**FIGURE 5.** (a) An illustration of the additional process step, and (b) a diffraction efficiency graph for the Ni-Ge zone plates.

The Ge etch has been done in a  $\text{CHF}_3$  plasma. A Cl-based plasma that had been developed for Ge zone plates [7] was initially used but a non-volatile thick compound was formed with the Ni during prolonged etching. Due to this problem, a  $\text{CHF}_3$ -based plasma-etch recipe was developed. The typical etch parameters are: 10-sccm gas flow, 3-mTorr pressure, and 50-W sample power. The resulting Ge etch rate with this recipe is 10 nm/min. The Ni structure is very resistant to the etching, and no degradation is observed. A small etch rate of 0.3 nm/min can be measured resulting in an etch selectivity between the Ni and Ge of 30:1.

Figure 6 shows SEM images of some of the results with the Ni-Ge process. In Fig. 6(a) a grating with 25-nm half-pitch, 60-nm Ni, and 150-nm Ge is shown. The interface between the Ni and Ge is difficult to see, but the small markers in the image indicate the position. Figures 6(b) and (c) show a fabricated Ni-Ge zone plate with  $dr_N = 30$  nm and with the same thicknesses as the grating in (a). Figure 6(d) shows a 16-nm half-pitch grating with 50-nm Ni and 50-nm Ge height that was possible to fabricate when the cold development process was used. Due to the excellent quality of the Ge etch, we believe that the only limitation is in the cold development and the Ni zone plate fabrication. This is promising for future work with this process.

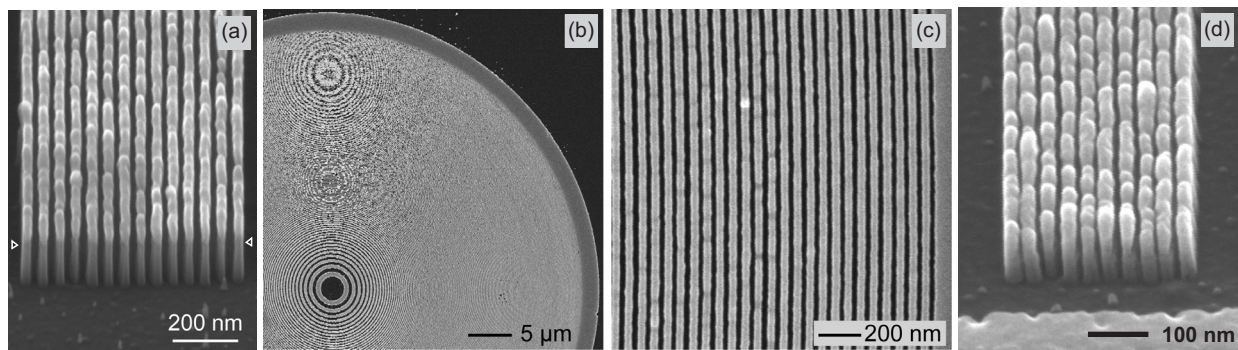


**FIGURE 6.** SEM images of gratings and a zone plate made with the Ni-Ge process.

The efficiency enhancement has been verified for zone plates with outermost zone widths down to 25 nm. The diffraction efficiency was measured at  $\lambda = 2.88$  nm. The measured efficiencies were between 10 and 11% for all zone plates with  $dr_N$  equal to 30 and 25 nm, and Ni and Ge thicknesses of  $\sim 57$  nm and 150 nm, respectively. This corresponds to over 70 % of the theoretical value at the given material heights, which is approximately the same fraction of the theoretical value as we have previously obtained for thick Ni zone plates. Furthermore, these efficiencies are about twice as high as the theoretical maximum for Ni zone plates with the same Ni thicknesses as the Ni-Ge zone plates had before the Ge etching.

## SUMMARY AND OUTLOOK

We have reported on our latest developments in nanofabrication methods and presented the recently fabricated zone plate optics. The improvement on the resist processing by cold development has resulted in fabricated Ni zone plates with  $dr_N = 13$  nm and a measured diffraction efficiency of  $2.4 \pm 0.4\%$ . The resolution in the resist pattern after cold development is down to 11-nm half-pitch. This is promising for fabricating narrower line widths after further refinement of the pattern transfer process. A fabrication process for Ni-Ge zone plates is presented. With this fabrication process the diffraction efficiency can be doubled compared to the corresponding standard Ni zone plate. In a proof-of-principle experiment the doubling of the efficiency was verified with zone plates with  $dr_N = 25$  nm. The higher-resolution capability of the Ni-Ge process has been demonstrated by showing a 16-nm half-pitch grating with 50-nm Ni and 50-nm Ge thicknesses, respectively.

In the near future we will continue to work with the Ni-Ge process. The high resolution that we have shown with cold development is, in combination with the excellent Ge etch, promising for fabricating zone plates with close to  $dr_N = 10$  nm. The fabricated zone plates will also be implemented in our laboratory soft x-ray microscope for imaging experiments.

## ACKNOWLEDGMENTS

The authors gratefully acknowledge the financial support of the Swedish Science Research Council, the Swedish Foundation for Strategic Research, the Wallenberg Foundation, and the Göran Gustafsson Foundation. The research leading to these results has also received funding from the European Community's Seventh Framework Programme (FP7/2007-2013) under grant agreement n° 226716.

## REFERENCES

1. C. Quitmann, C. David, F. Nolting, F. Pfeiffer, and M. Stampanoni, Eds., *J. Physics: Conf. Series* **186**, 011001 (2009).
2. W. Chao et al., *Opt. Express* **17**, 17669 (2009).
3. A. Holmberg, S. Rehbein, and H.M. Hertz, *Microelectron. Eng.* **73-74**, 639 (2004).
4. J. Reinspach et al., *J. Vac. Sci. Technol. B* **27**, 2593 (2009).
5. M. Bertilson, P. Takman, A. Holmberg, U. Vogt, and H. M. Hertz, *Rev. Sci. Instrum.* **78**, 026103 (2007).
6. M. Lindblom et al., *J. Vac. Sci. Technol. B* **27**, L5 (2009).
7. M. Lindblom et al., *J. Vac. Sci. Technol. B* **27**, L1 (2009).